

pubs.acs.org/JPCC Article

Thermodynamic and Structural Properties of Bulk and Thin-Film CeVO₄ and LaVO₄

Kai Shen, Jian Chang, Rajeev Kumar Rai, Ching-Yu Wang, Eric A. Stach, Raymond J. Gorte, and John M. Vohs*

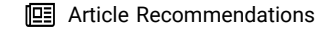


Cite This: J. Phys. Chem. C 2023, 127, 15591-15599



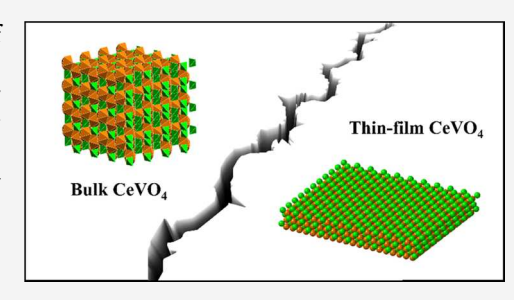
ACCESS I

III Metrics & More



SI Supporting Information

ABSTRACT: The thermodynamic and structural properties of 1 nm thick films of CeVO₄ and LaVO₄ supported on γ -Al₂O₃ were examined and compared to the corresponding bulk rare-earth vanadates. The films were prepared by atomic layer deposition (ALD) on high-surface-area powders and then examined after either oxidation or reduction at 1073 K. Both CeVO₄ and LaVO₄ uniformly covered the γ -Al₂O₃ in the form of two-dimensional crystallites. Thin-film LaVO₄ reversibly transitioned between a perovskite structure upon reduction to a monazite structure upon oxidation, similar to what is observed for the bulk material; however, coulometric titration (CT) showed that the P(O₂) at which equilibrium is established between these two phases was 7 orders of magnitude higher for the



thin-film material. Thin-film CeVO₄ also formed a perovskite phase upon reduction but reversibly transitioned to a fluorite phase upon oxidation rather than the zircon phase, which is formed for bulk CeVO₄. Multiple techniques showed that the oxidation states of both Ce and V in the thin-film CeVO₄ were +4, which is also different from bulk CeVO₄. Reasons for why the properties of the thin-film, rare-earth vanadates differ from their bulk counterparts are discussed.

1. INTRODUCTION

The rare-earth vanadates (REVO_x) are potentially of interest as oxidation catalysts and as supports for catalytic metals. For example, in the case of CeO₂-supported V₂O₅, vanadium can react with the underlying support to form the CeVO₄ at the interface, ¹ and this compound oxide has been identified as the active component for some oxidative dehydrogenation reactions ^{1,2} and for desulfurization and selective oxidation of H₂S. ^{3,4} CeVO₄ can also function as an "intelligent" catalyst support because its lattice can be doped with various transition metals, including Cu, Ni, and Co, ⁵ which can be reversibly "exsolved" from the lattice upon high-temperature reduction, potentially allowing large-metal particles to be redispersed. Finally, doped REVO_x can have high electronic conductivities, a property that is useful in some applications, such as in electrodes for solid-oxide electrochemical cells. ⁵

The redox properties of the various rare-earth vanadates are surprisingly similar. Thermodynamic measurements of LaVO₄-LaVO₃, CeVO₄-CeVO₃, and PrVO₄-PrVO₃ showed identical oxidation isotherms, with the phase transition occurring at an equilibrium P(O₂) of 10^{-18} atm at 973 K.⁶ Although Ce can exist in either the +3 or +4 oxidation state, Ce is locked into the +3-oxidation state in both the oxidized and reduced forms of CeVO_x, 7 partially explaining its similarity with LaVO_x. The bulk structures of CeVO_x and LaVO_x can be different, however. While the reduced forms, CeVO₃ and LaVO₃, both have a perovskite structure, in the oxidized forms, CeVO₄ and LaVO₄ exist as zircon and monazite structures, respectively. ⁸

Bulk rare-earth vanadates typically have surface areas that are too low for most catalytic applications. This is also a problem for many other bulk oxides. To circumvent this issue, our laboratories have been preparing high-surface-area metal oxides by depositing them as thin, conformal films on an inert high-surface-area support using atomic layer deposition (ALD). Because even relatively thin films result in high weight loadings (e.g., a 1 nm thick film of a material that has a bulk density of 5 g/cm³ on a 100 m²/g support will have a loading of 33 wt %), it is necessary for the oxide films to be less than 2 nm thick. Most of the ALD-grown oxide films that we have studied have formed two-dimensional crystallites, 11,12 and some exhibited properties that were different from that of their bulk counterparts. For example, high-temperature reduction of films with a CeMnO_x stoichiometry formed a stable perovskite structure, which has not been observed for the bulk material. 13 It was suggested that the stability of the two-dimensional crystallites is due either to interactions with the underlying support or to the effects of confining the film in two dimensions. In another example, thin films of CeFeO, were observed to reversibly transition from a fluorite structure

Received: May 16, 2023 **Revised:** July 11, 2023 **Published:** July 26, 2023





following oxidation to a perovskite structure following reduction, even though the corresponding bulk material irreversibly separated into ${\rm CeO_2}$ and ${\rm Fe_2O_3}$ phases following redox treatments. ¹⁴

In the present study, we set out to investigate CeVO_x films on γ -Al $_2\text{O}_3$ in order to understand the structure and redox thermodynamic properties of thin films with this composition. Because the properties of the oxidized CeVO_4 film were found to be very different from that of the bulk material, both in crystal structure and the oxidation states of the metal cations, we also examined the structure and equilibrium thermodynamics of LaVO_x films in order to determine the effect of the rare-earth cations on these properties.

2. EXPERIMENTAL SECTION

The CeVO_x and LaVO_x films used in this study were deposited by ALD using equipment and procedures that have been described in detail elsewhere. Briefly, ~0.5 g of the substrate was first heated in vacuum, then exposed to the precursor vapor pressure for 5 min. After evacuation to remove excess precursor, the sample was removed from the system and calcined in a muffle furnace at 823 K for 5 min to remove the precursor ligands. The sample was then placed back into the system, and the procedure was repeated for the desired number of cycles. The ALD precursors for Ce, La, and V were $Ce(TMHD)_4$ (TMHD = 2,2,6,6-tetramethyl-3,5-heptanedionato), La(TMHD)₃, and VO(acac)₂ (vanadium(IV)bis-(acetylacetonato)oxide), all purchased from Strem Chemicals, Inc., with purities of 97, 99, and 98%, respectively. The substrate temperature during exposure to the precursors was 543 K for Ce(TMHD)₄ and La(TMHD)₃, and 453 K for VO(acac)₂. The growth rates for each precursor were measured gravimetrically and found to be 4.0×10^{17} Ce atoms m⁻² cycle⁻¹, 5.6 \times 10¹⁷ La atoms m⁻² cycle⁻¹, and 8.8 \times 10¹⁷ V atoms m⁻² cycle⁻¹.

The CeVO₄ films were deposited directly onto γ-Al₂O₃ (Strem Chemicals, Inc.) that had been calcined at 1173 K for 24 h and had a Brunauer-Emmett-Teller (BET) surface area of 125 m² g⁻¹. To form films having the correct Ce:V stoichiometry, every V ALD cycle was followed by either two or three Ce ALD cycles. Because La can react with γ -Al₂O₃ to form LaAlO₃, the γ -Al₂O₃ support was first modified by wet infiltration with 15 wt % CaO to form a barrier layer. La and V ALD cycles were again alternated so as to achieve the correct La:V stoichiometry. The sample with a CeVO₄ film had a loading of 38.9 wt % CeVO₄ on the γ -Al₂O₃ support, while the sample with the LaVO₄ had a loading of 25.4 wt % LaVO₄ film on CaO-γ-Al₂O₃ support. In both cases, the films were nominally 1 nm thick, assuming they covered the substrates uniformly and had the same densities as the corresponding bulk materials. After the films were deposited, the samples were subjected to five redox cycles, each consisting of reduction in flowing 10% H₂-He mixtures for 6 h at 1073 K, followed by oxidation in air for 2 h at 1073 K.

Bulk CeVO₄ and LaVO₄ samples were also prepared for comparison purposes. The synthesis procedure for these materials consisted of mixing an aqueous solution of 1 g of ammonium metavanadate (NH₄·VO₃, Sigma-Aldrich, 99%) together with 2 g of citric acid (Fisher Chemical, 99.5%) and stoichiometric amounts of either cerium(III) nitrate hexahydrate (Ce(NO₃)₃·6H₂O, Alfa Aesar, 99%) or lanthanum(III) nitrate hexahydrate (La(NO₃)₃·6H₂O, Alfa Aesar, 99%). The

resulting solutions were heated to ${\sim}423~{\rm K}$ to evaporate the liquid and then calcined in air at 1073 K for 12 h.

BET surface areas were obtained from N2 adsorption isotherms measured at liquid nitrogen temperature on a home-built apparatus. X-ray diffraction (XRD) patterns were collected with a Rigaku MiniFlex diffractometer, employing a Cu K α source (λ = 0.15416 nm) and a HyPix-400 MF (2D) HPAD) detector. High-resolution transmission electron microscopy (HR-TEM) images were obtained using a JEOL JEM-F200 operated at 200 kV. Electron energy loss spectroscopy (EELS) spectra, along with high-angle annular dark-field scanning transmission electron microscopy (HAADF-STEM) images and energy-dispersive X-ray spectroscopy (EDS) mappings, were acquired using an aberration-corrected JEOL NEOARM, operated in STEM mode at 200 kV. EELS measurements were performed with a Gatan Image Filter which integrates DualEELS capability to ensure precise energy calibration and a K2-IS direct electron detector at the end of the filter. For ex situ microscopy, the powders were mixed with ethanol and then deposited onto a lacey carbon film on copper grids (Electron Microscopy Sciences). X-ray photoelectron spectra (XPS) were obtained using a physical electronics versaProbe 5000 X-ray photoelectron spectrometer with a monochromatic 1486.2 eV Al K- α source. The XPS chamber had a base pressure of 3×10^{-7} Pa (ultrahigh vacuum) before the samples were transferred. During data acquisition, the pressure was 1.6×10^{-6} Pa. A Shirley-type background was subtracted from each XPS spectrum. X-ray-absorption nearedge structure (XANES) spectra at the Ce L₃ edge were collected using an easy XAFS300 (easy XAFS LLC), equipped with a Si (211) analyzer. Raman measurements were carried out with a laser power of 1 mW at the sample and an exposure time of 240 s.

The oxygen stoichiometries and oxidation isotherms for the CeVO_x and LaVO_x films were measured as a function of $\text{P(O}_2)$ at 1073 K using coulometric titration (CT). ¹⁶ For these measurements, ~0.25 g of sample was placed in the middle of YSZ (yttria-stabilized zirconia) tube that had Pt electrodes painted on the inner and outer surfaces. The YSZ tube and sample were then heated to 1073 K at 1 K/min while flowing a mixture of 10% H_2 and 3% H_2O in He over the sample. When the sample reached 1073 K, the ends of the tube were sealed, and the two electrodes were connected to a potentiostat (Gamry Instruments, Inc.). The P(O_2) inside the tube could then be determined from the open-circuit voltage (OCV) across two electrodes, using the Nernst equation. Precise amounts of oxygen could be added or removed from inside the tube by applying a current across the electrodes.

Flow titration was also used to measure the oxygen uptake by the reduced samples. In these experiments, 200 mg of sample was first reduced in 100 mL/min flow of a 10% $\rm H_2\textsc{-}He$ mixture for 6 h at 1073 K. The sample was then reoxidized in a flowing stream of 10% air in He at the same temperature. During oxidation, the $\rm N_2$ and $\rm O_2$ signals were recorded by an online mass spectrometer, and the $\rm O_2$ uptake by the reduced sample was determined by integrating the difference between these two signals.

3. RESULTS

The surface areas of the bulk and thin-film, CeVO₄, and LaVO₄ samples are shown in Table 1, together with those of the bare supports. Both thin-film samples were reduced and oxidized five times at 1073 K prior to these measurements. The surface

Table 1. Summary of Physical Characteristics of the Samples Investigated in This Study

	oxide loadings (wt %)	BET areas (m^2/g)
γ -Al ₂ O ₃		125
$CaO-\gamma-Al_2O_3$	15.0	71
$CeVO_4/\gamma$ - Al_2O_3	38.9	56
bulk CeVO ₄		<1
$LaVO_4/CaO-\gamma-Al_2O_3$	25.4	42
bulk LaVO ₄		<1

areas of the bulk samples were too low to accurately measure but were less than 1 $\rm m^2/g$. By contrast, the two thin-film samples had surface areas of 56 and 42 $\rm m^2/g$, respectively. The weight loadings of CeVO₄ and LaVO₄ on the thin-film samples were chosen to produce films that were 1 nm thick, assuming that the films uniformly covered the surfaces of the supports and that the density of the films was equal to the bulk densities of their corresponding rare-earth vanadates. The decrease in specific surface areas of the thin-film samples compared to the supports used in making those samples is primarily due to the increase in mass associated with the films.

3.1. Film Structure. The XRD patterns for bulk CeVO₄ and CeVO₄/ γ -Al₂O₃ are shown in Figure 1 following either oxidation or reduction at 1073 K. The data for the oxidized bulk sample, Figure 1a, corresponds to a zircon structure, while the pattern for the reduced sample corresponds to a perovskite structure. For the thin film, the nominal thickness of 1 nm is close to the coherence length of the X-rays, intense diffraction peaks were still observed following either oxidation or reduction. The diffraction patterns for CeVO₄/γ-Al₂O₃, however, are not identical to those of the bulk sample. Features associated with the CeVO_x phases overwhelmed the small features associated with the γ -Al₂O₃ support; and, based on the peak widths at half-maximum, the average crystallite sizes were about 10 nm for both the oxidized and reduced samples. More importantly, while CeVO_x in the reduced sample was similar to that of the bulk in forming a perovskite structure, the diffraction pattern of the oxidized sample showed a fluorite structure, similar to that of bulk CeO₂. A Raman spectrum of this sample is presented in Figure S1 and is dominated by a peak at 460 cm⁻¹, which is characteristic of a fluorite CeO2 lattice. The spectrum also contains some minor peaks at 280, 800, and 860 cm⁻¹, which can be assigned to

tetrahedral $\mathrm{VO_4}$ bending or stretching modes. The spectrum does not, however, contain peaks characteristic of $\mathrm{V_2O_5}$. Together the XRD and Raman results indicate that the ceria and vanadia have not separated into different oxide phases. Also, if this had occurred, the transition from fluorite to perovskite structures should not be completely reversible upon oxidation and reduction. Thus, the vanadium atoms appear to be substituted into the fluorite lattice or remain closely associated with the ceria.

The analogous diffraction results for the LaVO_x samples are shown in Figure 2. Again, results for the oxidized and reduced forms of bulk LaVO₄ in Figure 2a are identical to what has been reported previously for the bulk material, ¹⁷ with LaVO₄ forming a monazite structure and LaVO₃ a perovskite structure. As shown in Figure 2b, the thin-film, LaVO₄/ CaO/ γ -Al₂O₃ sample again exhibited a reversible phase transition upon oxidation or reduction; however, unlike CeVO_x, the oxidized and reduced forms of thin-film, LaVO₄ exhibited identical structures to that found for the bulk material, with the oxidized sample again showing a monazite structure and the reduced sample exhibiting a perovskite structure. Based on the peak widths, the crystallite sizes for the oxidized and reduced samples were 8 and 9 nm, again significantly larger than the nominal film thickness.

HAADF-STEM images and EDS mappings for V, Ce, and Al are shown in Figure S2a,b for the oxidized and reduced $\text{CeVO}_{x}/\gamma\text{-Al}_{2}\text{O}_{3}$ samples. On the magnification used here, the microscopy images are indistinguishable from that of the γ -Al₂O₃ support, implying that there are no large crystallites of the deposited oxides, even though the loading of CeVO_x is high. Also, the EDS maps indicate that the signals for Ce, V, and Al are strongly correlated, implying that the CeVO_x film uniformly covers the entire surface of the γ -Al₂O₃ support. The fact that the film remained conformal with the support, even after five reduction and oxidation cycles may suggest there are attractive interactions between the $CeVO_x$ and γ -Al₂O₃. The analogous HAADF-STEM images and EDS maps for V, La, and Al in the oxidized and reduced LaVO₄/CaO/γ-Al₂O₃ sample are shown in Figure S3. These results again demonstrate that the film uniformly covers the support.

HR-TEM images of the oxidized and reduced CeVO_x/γ -Al₂O₃ sample are shown in Figure 3a,b and provide additional information on the structure of the CeVO_x film. The insets in each image correspond to the fast Fourier transform (FFT)

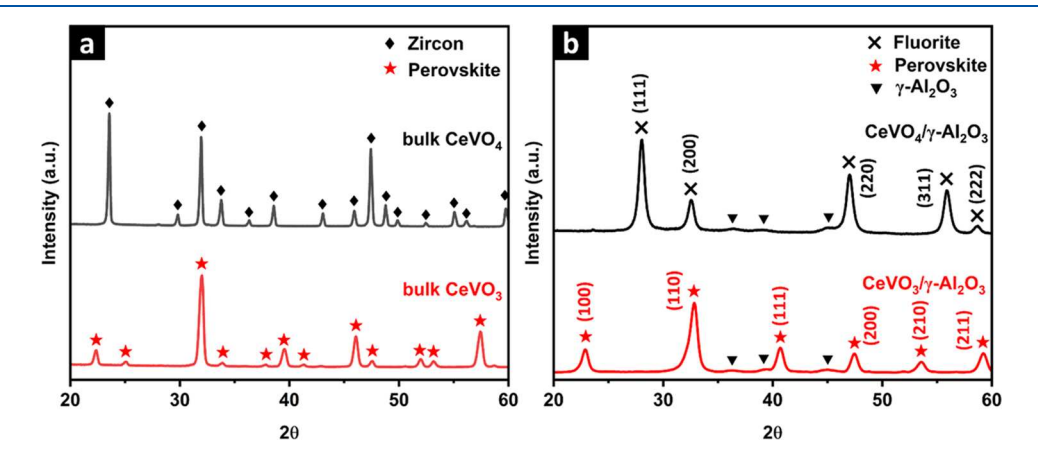


Figure 1. XRD patterns of (a) bulk CeVO₄ and (b) CeVO_x/ γ -Al₂O₃ samples oxidized in dry air (black) and reduced in 10% H₂/He (red) at 1073 K.

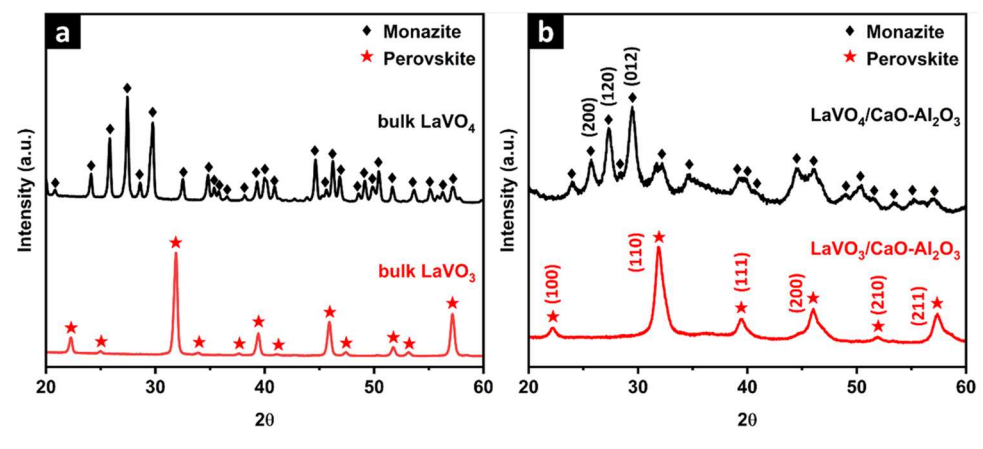


Figure 2. XRD patterns of (a) bulk LaVO₄ and (b) LaVO_x/CaO/ γ -Al₂O₃ samples oxidized in dry air (black) and reduced in 10% H₂/He (red) at 1073 K.

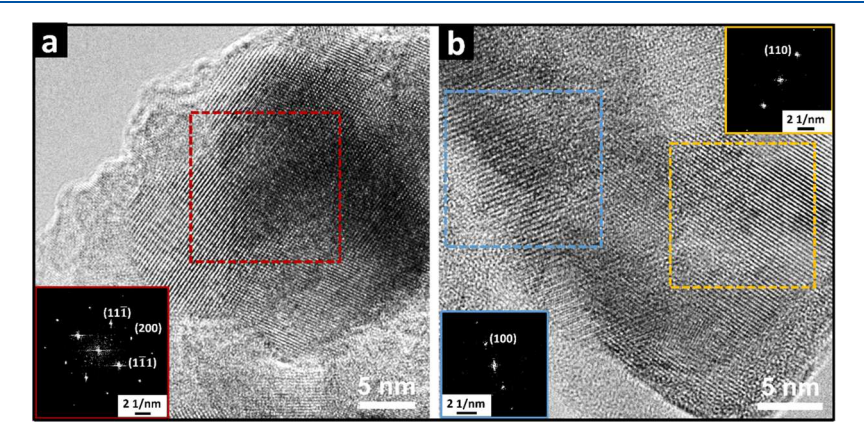


Figure 3. HR-TEM images of (a) the dry-air-oxidized and (b) 10% H_2/He -reduced $CeVO_x/\gamma - Al_2O_3$ at 1073 K.

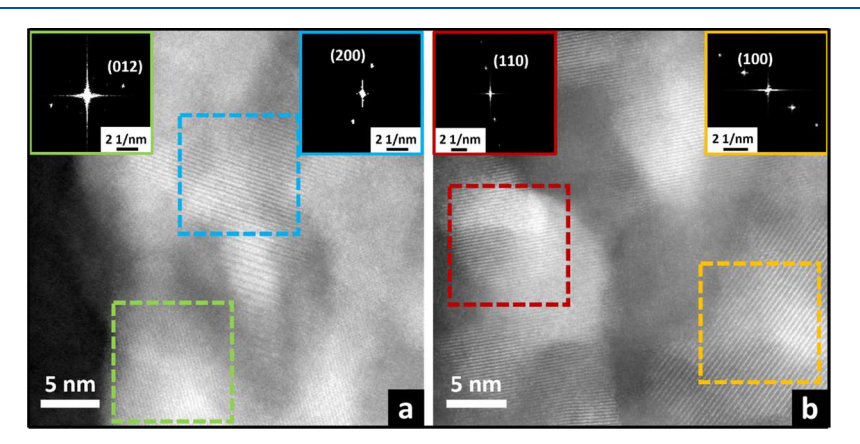


Figure 4. HR-STEM images of (a) the dry-air-oxidized and (b) 10% H₂/He-reduced LaVO_x/CaO/γ-Al₂O₃ at 1073 K.

diffractograms of the indicated regions. Both images show lattice fringes that are not present for the bare γ -Al₂O₃ and can therefore be attributed to the CeVO_x film. The image in Figure 3a contains lattice fringes over most of the surface. The domain size of the fringes in the image is roughly 10 nm, in good agreement with the crystal-size estimate from the XRD peak width. The fringes in Figure 3a are also consistent with the fluorite features in the XRD patterns and the FFT shows peaks corresponding to the (200) and (111) planes of that phase. Figure 3b presents two sets of lattice fringes for the reduced CeVO_x film, with *d*-spacings of 3.92 and 2.74 nm that

can be assigned to the (100) and (110) planes of a perovskite phase.

HR-STEM images of the oxidized and reduced LaVO_x/CaO- γ -Al₂O₃ sample are shown in Figure 4. Again, well-defined lattice fringes associated with the LaVO₄ films are clearly visible. The *d*-spacing in FFT diffractograms for the oxidized sample in Figure 4a, are characteristic of the (012) and (200) planes of the monazite structure. Similarly, the reduced sample in Figure 4b shows spacings characteristic of the (110) and (100) planes of the perovskite phase. Most of the surface is covered by the films and the domain size of the two-dimensional crystallites is ~10 nm.

3.2. Cation Oxidation States. Literature sources indicate that in the oxidized form of bulk CeVO₄, Ce is in the +3-oxidation state and V is +5. Furthermore, theoretical considerations have suggested that Ce cannot be oxidized to the +4 oxidation state in CeVO₄, in large part because of the structure. In a DFT study, Da Silva et al. showed that Ce⁴⁺ is stabilized relative to Ce³⁺ in the fluorite structure by the orientation of the Ce–O bonds, which are different in the zircon structure. Given that the oxidized CeVO₄ in the CeVO_x/ γ -Al₂O₃ sample forms a fluorite structure, it is interesting to ask whether the oxidation states of the metal cations in the thin-film sample may be different from that of bulk material.

EELS spectra of the Ce $M_{4,5}$ edges and V $L_{2,3}$ edges for the oxidized and reduced $CeVO_x/\gamma$ -Al $_2O_3$ samples are shown in Figure 5. As expected, the spectrum for the reduced sample,

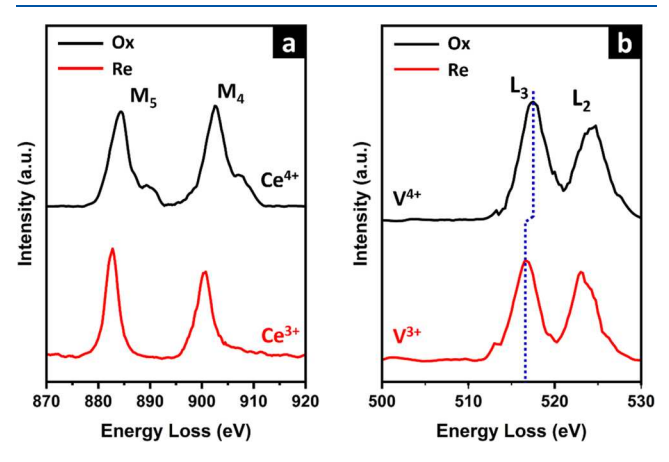


Figure 5. EELS spectra of (a) the Ce $M_{4,5}$ edges and (b) the V $L_{2,3}$ edges of the oxidized and reduced $\text{CeVO}_x/\gamma\text{-Al}_2\text{O}_3$. The sample was pretreated by 5 redox cycles followed by oxidation or reduction in dry air or hydrogen at 1073 K to obtain the oxidized or reduced state.

Figure 5a, demonstrates that Ce is in the +3-oxidation state, with M₅ and M₄ edges at 882.8 and 900.7 eV, respectively. Upon oxidation, the cerium cations are fully oxidized to Ce⁴⁺ as demonstrated by the shift of M_{4,5} edges to 884.4 and 902.8 eV, along with the appearance of two satellite peaks at 890.0 and 907.5 eV. 19 The V edge data in Figure 5b show the V L₃ and L₂ edges at 516.7 and 523.3 eV for the reduced sample. These peak positions are characteristic of V^{3+20} Upon oxidation, the spectrum shifts approximately 0.8 eV to higher energy loss, suggesting the formation of V⁴⁺ cations.²¹ The result for vanadium in the oxidized sample is somewhat surprising, given V5+ is normally observed for fully oxidized vanadia. However, the EELS results are consistent with the thin-film $CeVO_4$ having Ce^{4+} and V^{4+} cations in a fluorite lattice, rather than Ce³⁺ and V⁵⁺ as reported for the bulk zircon phase.

The XPS spectra in Figure 6 provide further evidence for these conclusions. Figure 6a shows the $Ce(3d_{3/2})$ and $Ce(3d_{5/2})$ regions for the oxidized and reduced $CeVO_x/\gamma$ -Al₂O₃ samples. The spectrum of the oxidized sample features three $3d_{5/2}-3d_{3/2}$ doublets, denoted as u/v, u''/v'', and u'''/v''', which are characteristic of Ce^{4+} cations.²²⁻²⁴ The u''''/v''' doublet centered at 916.3 and 898.2 eV is due to the primary photoemission of Ce^{4+} , with two separate shake-down satellite features, u-v and u''-v'' doublets, located at 900.5 and 882.1 eV, and at 907.0 and 885.3 eV, respectively. This is consistent

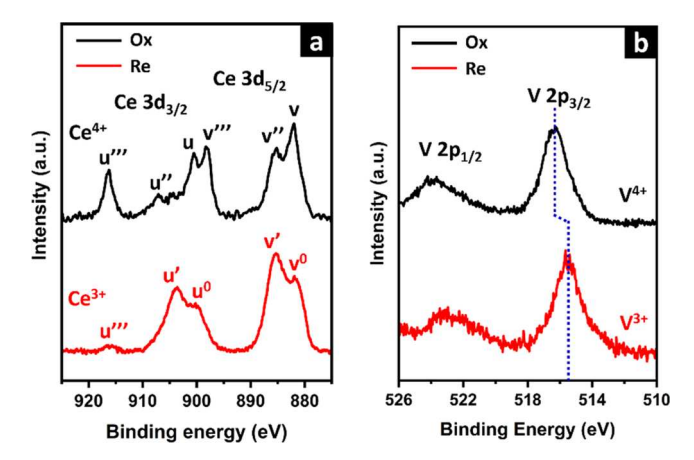


Figure 6. XPS spectra of (a) the Ce 3d regions and (b) the V 2p regions of the oxidized and reduced $\text{CeVO}_x/\text{g-Al}_2\text{O}_3$. The sample was pretreated by 5 redox cycles followed by oxidation or reduction in dry air or hydrogen at 1073 K to obtain the oxidized or reduced state.

with the EELS results that Ce cations in the thin-film CeVO₄ are of +4 oxidation states. For the reduced sample, the spectrum is mainly composed of two $3d_{3/2}-3d_{5/2}$ doublets, where the u'/v' doublet at 903.6 and 885.3 eV are the primary photoemission peaks, with the shake-down u^0/v^0 doublet at 900.4 and 881.8 eV. The spectrum is in agreement with that previously documented for Ce³⁺. ^{22,23} A small peak for Ce⁴⁺ is also present in this spectrum at 916.4 eV but is estimated to account for only ~1% of Ce cations in the sample.

The $V(2p_{1/2})$ and $V(2p_{3/2})$ regions for the oxidized and reduced $CeVO_x/\gamma$ -Al $_2O_3$ samples are shown in Figure 6b. The spectrum of the reduced sample is that of V^{3+} , with $2p_{1/2}$ and $2p_{3/2}$ peaks at 523.1 and 515.6 eV, respectively. Upon oxidation, both peaks upward shift by 0.8 eV to positions consistent with that expected for V^{4+} . This again coincides with the EELS results. A summary of XPS results is provided in Table 2.

Table 2. Summary of XPS Results

	dominant peak positions		
	oxidized CeFeO _x /γ-Al ₂ O ₃	reduced CeFeO _x /γ-Al ₂ O ₃	
Ce (3d _{3/2})	u"' at 916.3 eV	u' at 903.6 eV	
Ce $(3d_{5/2})$	v''' at 898.2 eV	ν' at 885.3 eV	
$V(2p_{1/2})$	523.9 eV	523.1 eV	
$V(2p_{3/2})$	516.4 eV	515.6 eV	
cation oxidation states	Ce ⁴⁺ , V ⁴⁺	mainly Ce ³⁺ , V ³⁺ with trace amount of Ce ⁴⁺	

That Ce changes oxidation states upon oxidation and reduction of the $\text{CeVO}_x/\gamma\text{-Al}_2\text{O}_3$ sample is further shown by the XANES results for the Ce L₃ edge displayed in Figure 7. For the reduced sample, the primary edge at 5728.9 eV demonstrates that the majority of Ce atoms are in the +3-oxidation state. The small edge at 5739.8 eV indicates the presence of a small amount of Ce^{4+} , possibly due to exposure of the sample to air prior to analysis. For the oxidized film, the Ce cations are all in the +4-oxidation state, as indicated by the characteristic Ce^{4+} doublet at 5733.4 and 5740.3 eV.

It is interesting to compare these results to those for the $LaVO_x/CaO-\gamma-Al_2O_3$ sample. As shown in Figure 8a, the EELS spectrum of V in the reduced $LaVO_x/CaO-\gamma-Al_2O_3$ sample

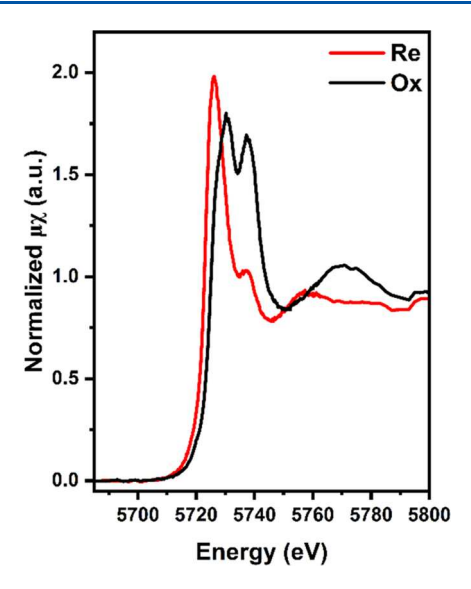


Figure 7. XANES spectra at Ce L₃ edge of the reduced (red) and oxidized (black) $\text{CeVO}_x/\gamma\text{-Al}_2\text{O}_3$ samples.

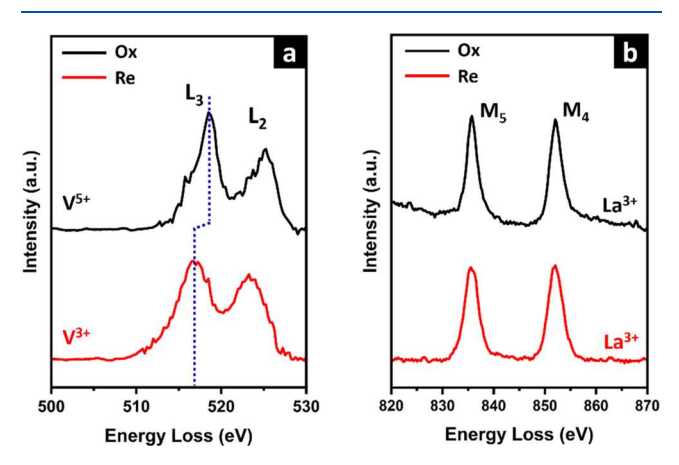


Figure 8. EELS spectra of (a) the V $L_{2,3}$ edges and (b) the La $M_{4,5}$ edges of the oxidized and reduced LaVO_x/CaO-γ-Al₂O₃. The sample was pretreated by 5 redox cycles followed by oxidation or reduction in dry air or hydrogen at 1073 K to obtain the oxidized or reduced state.

shows L_3 and L_2 edges at 516.7 and 523.3 eV, respectively, indicating V cations are in the +3-oxidation state. Upon calcining in air at 1073 K, both L_3 and L_2 edges shift 1.8 eV to higher loss energies, indicating the formation of the expected V^{5+} . The much larger shift observed here for the LaVO₄ film compared to what was observed with CeVO₄ helps confirm that V is in the +4 oxidation state in the CeVO₄ film. As expected, the EELS spectra of La in the oxidized and reduced samples are the same, with both showing M_5 and M_4 edges at 835.7 and 851.9 eV, respectively, implying that La cations remain in the +3-oxidation state.

3.3. Redox Thermodynamics. For both $CeVO_x$ and $LaVO_x$, the oxygen stoichiometry (i.e., value of x) as a function of $P(O_2)$ at a constant temperature has previously been measured. Data obtained at 973 K for these oxides are reproduced in Figure S4. These data show that both oxides undergo an equilibrium phase change from REVO₄ to an REVO₃ at a well-defined $P(O_2)$ of 10^{-19} atm for $CeVO_4$ — $CeVO_3$ and 10^{-18} atm for $LaVO_4$ — $LaVO_3$. Using the measured oxidation enthalpies, these values will shift to 10^{-15} and 10^{-14} atm at 1073 K. The analogous results for the $CeVO_x/\gamma$ - Al_2O_3

and $LaVO_x/CaO-\gamma-Al_2O_3$ samples at 1073 K are shown in Figure 9. Consistent with the bulk materials, these data and the

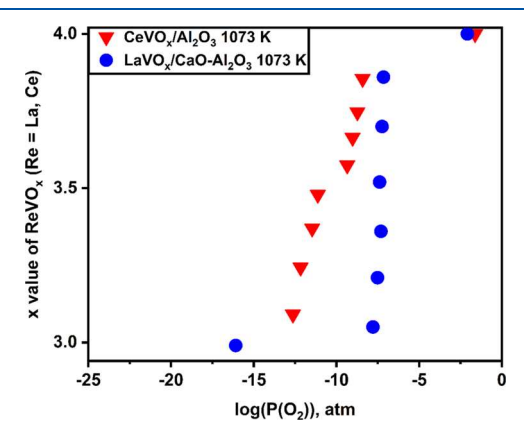


Figure 9. CT results of $\text{CeVO}_x/\gamma\text{-Al}_2\text{O}_3$ at 973 K (black triangle) and 1073 K (red triangle) and $\text{LaVO}_x/\text{CaO-}\gamma\text{-Al}_2\text{O}_3$ (blue circle) at 1073 K

flow titration results described below, show that the amount of oxygen removed in going from the oxidized sample to the reduced sample corresponds to one oxygen atom per V in both cases; however, the equilibrium $P(O_2)$ values vary significantly for the two vanadates.

For the LaVO $_x$ /CaO- γ -Al $_2$ O $_3$ sample, the equilibrium P(O $_2$) of the phase transition is well defined and occurs at a P(O $_2$) of 10^{-7} atm at 1073 K. While all of the data described above indicate that the structures of the oxidized and reduced LaVO $_x$ film were the same as those of the bulk material, it is noteworthy that the phase transition for the thin film occurs at a P(O $_2$) which is 7 orders of magnitude higher than that of the bulk oxide. This demonstrates that the energetics of the phase transition are significantly different for these two forms of the oxide. Whether this is due to interactions with the support or to the high, surface-to-bulk ratio of the thin film is not clear, but the change in ΔG of reaction is significant.

The equilibrium $P(O_2)$ for the phase transition in the $CeVO_x/\gamma$ -Al₂O₃ sample also shifted to a much higher value compared to that for the bulk oxide (Figure 9). In this case, the $P(O_2)$ changes more gradually as the sample is oxidized or reduced and there is a hint of an inflection point at an oxygen stoichiometry of 3.5. Since both Ce and V are undergoing changes in their oxidation state, from Ce^{4+} to Ce^{3+} and V^{4+} to V^{3+} , it is possible this inflection point is associated with formation of $Ce^{3+}V^{4+}O_{3.5}$ or $Ce^{4+}V^{3+}O_{3.5}$; however, it was not possible for us to stabilize the material at this intermediate oxidation state precluding the characterization of the cation oxidation states at this point in the phase transition.

To further confirm the oxygen stoichiometry in the reduced thin-film samples, flow titration measurements were performed for both $\text{CeVO}_x/\gamma\text{-Al}_2\text{O}_3$ and $\text{LaVO}_x/\text{CaO-}\gamma\text{-Al}_2\text{O}_3$. In these experiments, the sample was initially reduced in 10% H₂-He at 1073 K and then reoxidized in a flowing 10% air-He stream with the oxygen uptake determined using an online mass spectrometer. For both samples, these experiments showed that the reduction procedure resulted in the removal of one oxygen atom per V from the fully oxidized sample, which is consistent with CT measurements.

4. DISCUSSION

The results obtained here demonstrate that thin films of rareearth vanadates can exhibit different structures and thermodynamic properties compared to their bulk counterparts. For Al_2O_3 -supported $CeVO_4$ and CaO/Al_2O_3 -supported $LaVO_4$, the equilibrium $P(O_2)$ associated with the $REVO_4$ -REVO_3 phase transition is shifted to much higher values than those for the bulk oxides, implying that the magnitude of $\Delta G_{\text{oxidation}}$ is significantly lower for oxidation of the thin films. In the case of $CeVO_4$, both the structure and the oxidation states of the Ce and V cations were different for the oxidized thin films. These changes could have important implications for a wide variety of applications. For catalysts, the change in $\Delta G_{\text{oxidation}}$ is expected to have a dramatic effect on any oxidation reaction. Similarly for chemical looping applications, the ability to release oxygen at lower temperatures will change the required process conditions.

There are several possible reasons for why the properties of thin films are so different than those of the bulk oxides. The most likely factor is the surface energy associated with terminating the crystal. Similar effects have been reported for nanostructured materials. For example, a theoretical study to minimize the energy of Ce_nO_{2n} clusters as a function of n using a simple interatomic potential showed that the fluorite structure only formed for n greater than about 50.30 The reason for this is that the atoms at the surface are undercoordinated relative to those in the bulk. Given that the films in our study were only 1 nm thick (roughly the thickness of two unit cells), the majority of the atoms will be present at either the interface with the support oxide or on the surface. Bonding interactions with support oxide could also be important so that the properties could change with the support composition. One would obviously expect the properties of the film to change with thickness, approaching bulk properties for very thick films. Unfortunately, it is not possible to ascertain such effects using the high-surface-area thin-film samples used in this study. As noted above, the 1 nm $\text{CeVO}_4/\gamma\text{-Al}_2\text{O}_3$ sample was already 38.9 wt % CeVO₄ and pore blocking would quickly become an issue for thicker films.

The observation that both Ce and V exist in the +4-oxidation state in the oxidized $CeVO_4$ film is particularly noteworthy. As pointed out earlier, Ce^{4+} is stabilized relative to Ce^{3+} in the fluorite structure due to the tetrahedral coordination of the cations in this lattice. Therefore, the formation of Ce^{4+} in the thin-film $CeVO_4$ is likely related to the fact that the films formed a fluorite structure. Stabilization of V^{4+} relative to V^{5+} implies that the V cations remain in the same phase with Ce since V^{5+} would almost certainly form under oxidizing conditions if there were phase separation. It is possible that the V^{4+} ions are in cation positions of the fluorite lattice. The fact that both Ce and V undergo changes in their oxidation states suggests that these thin-film materials could have interesting electronic and optical properties.

The photoactivities of CeVO₄ have been explored in a number of studies, primarily focusing on applications such as the control of organic pollutants and ammonia reduction. Since these studies have used bulk forms of CeVO₄, which have a zircon structure with Ce³⁺ and V⁵⁺ cations, the photoactivities of the thin-film CeVO₄/ γ -Al₂O₃ may be substantially different and therefore warrant further investigation.

Finally, based on the results obtained in this study for rareearth vanadates, one might expect other oxide films to have crystal structures and thermodynamic redox properties that vary from that of the bulk oxides. Thus, changing in the morphology of a material, e.g., using a thin film rather than a bulk powder, could provide a means to tailor properties for specific applications. This concept is relatively unexplored but could lead to new materials with important properties.

5. CONCLUSIONS

This study reveals that the thin-film rare-earth vanadates exhibit properties that are significantly different from their bulk analogues. Equilibrium constants for the reduction of Al₂O₃-supported, thin films of CeVO₄ and LaVO₄ differ significantly from that of the bulk materials. In the case of CeVO₄, the thin films showed a different structure, fluorite rather than zircon, and had Ce and V in different oxidation states. The results suggest that thin-film oxides may possess attributes that greatly deviate from their bulk counterparts, making them compelling candidates for a range of applications from thermoto photocatalysis.

ASSOCIATED CONTENT

Supporting Information

The Supporting Information is available free of charge at https://pubs.acs.org/doi/10.1021/acs.jpcc.3c03240.

Raman spectrum of the oxidized $\text{CeVO}_x/\gamma\text{-}\text{Al}_2\text{O}_3$ (Figure S1); high-angle annular dark-field scanning transmission electron microscopy (HAADF-STEM) images and the corresponding EDS mappings for $\text{CeVO}_x/\gamma\text{-}\text{Al}_2\text{O}_3$ (Figure S2); HAADF-STEM images and the corresponding EDS mappings for $\text{LaVO}_x/\text{CaO}/\gamma\text{-}\text{Al}_2\text{O}_3$ (Figure S3); and CT results of bulk CeVO_x and LaVO_x (Figure S4) (PDF)

AUTHOR INFORMATION

Corresponding Author

John M. Vohs — Department of Chemical and Biomolecular Engineering, University of Pennsylvania, Philadelphia, Pennsylvania 19104, United States; orcid.org/0000-0002-8283-5241; Email: vohs@seas.upenn.edu

Authors

Kai Shen – Department of Chemical and Biomolecular Engineering, University of Pennsylvania, Philadelphia, Pennsylvania 19104, United States

Jian Chang — Department of Chemical and Biomolecular Engineering, University of Pennsylvania, Philadelphia, Pennsylvania 19104, United States; orcid.org/0000-0002-8618-292X

Rajeev Kumar Rai — Department of Materials Science and Engineering, University of Pennsylvania, Philadelphia, Pennsylvania 19104, United States; oorcid.org/0000-0002-2248-7601

Ching-Yu Wang — Department of Chemical and Biomolecular Engineering, University of Pennsylvania, Philadelphia, Pennsylvania 19104, United States

Eric A. Stach — Department of Materials Science and Engineering, University of Pennsylvania, Philadelphia, Pennsylvania 19104, United States; orcid.org/0000-0002-3366-2153

Raymond J. Gorte — Department of Chemical and Biomolecular Engineering, University of Pennsylvania, Philadelphia, Pennsylvania 19104, United States; orcid.org/0000-0003-0879-715X

Complete contact information is available at: https://pubs.acs.org/10.1021/acs.jpcc.3c03240

Notes

The authors declare no competing financial interest.

ACKNOWLEDGMENTS

This work was supported by the Air Force Office of Scientific Research, under AFOSR Award No. FA9550-19-1-0326. Some of the work was performed at the Singh Center for Nanotechnology at the University of Pennsylvania, a member of the National Nanotechnology Coordinated Infrastructure (NNCI) network, which is supported by the National Science Foundation (Grant NNCI-2025608). The authors gratefully acknowledge support of the Nanoscale Characterization Facility at the Singh Center by the NSF through the University of Pennsylvania Materials Research Science and Engineering Center (MRSEC) (DMR-1720530) and the NSF Major Research Instrumentation Program (CHE-2117783) and the University of Pennsylvania for supporting the purchase of the easyXAFS300 spectrometer that was used in this study. The authors thank Materials Characterization Core at Drexel University and Dr. Dmitri Barbash for assistance with XPS experiments and analysis. They also thank Ryan Murphy and Dr. Neil Tomson for their assistance and useful discussion on XANES experiments.

REFERENCES

- (1) Martínez-Huerta, M. V.; Deo, G.; Fierro, J. L. G.; Banares, M. A. Changes in ceria-supported vanadium oxide catalysts during the oxidative dehydrogenation of ethane and temperature-programmed treatments. *J. Phys. Chem. C* **2007**, *111*, 18708–18714.
- (2) Ganduglia-Pirovano, M. V.; Popa, C.; Sauer, J.; Abbott, H.; Uhl, A.; Baron, M.; Stacchiola, D.; Bondarchuk, O.; Shaikhutdinov, S.; Freund, H. J. Role of Ceria in Oxidative Dehydrogenation on Supported Vanadia Catalysts. *J. Am. Chem. Soc.* **2010**, *132*, 2345–2349.
- (3) Li, X. Y.; Shi, J. J.; Wang, J. A.; Xi, L.; Sun, R.; Zhang, F.; Wu, X.; Zhou, Z. Y.; Ren, Z. Q. Preparation of CeVO₄/BNNS catalyst and its application in oxidation desulfurization of diesel oil. *Fuel* **2023**, 337, 126875.
- (4) Yasyerli, S.; Dogu, G.; Dogu, T. Selective oxidation of H₂S to elemental sulfur over Ce-V mixed oxide and CeO₂ catalysts prepared by the complexation technique. *Catal. Today* **2006**, *117*, 271–278.
- (5) Adijanto, L.; Padmanabhan, V. B.; Kungas, R.; Gorte, R. J.; Vohs, J. M. Transition metal-doped rare earth vanadates: a regenerable catalytic material for SOFC anodes. *J. Mater. Chem.* **2012**, 22, 11396–11402.
- (6) Adijanto, L.; Padmanabhan, V. B.; Holmes, K. J.; Gorte, R. J.; Vohs, J. M. Physical and electrochemical properties of alkaline earth doped, rare earth vanadates. *J. Solid State Chem.* **2012**, *190*, 12–17.
- (7) Reidy, R. F.; Swider, K. E. Determination of the Cerium Oxidation-State in Cerium Vanadate. *J. Am. Ceram. Soc.* **1995**, 78, 1121–1122.
- (8) Yoshimura, M.; Sata, T. A New Monoclinic Phase of Cerium Orthovanadate (CeVO₄). Bull. Chem. Soc. Jpn. 1969, 42, 3195–3198.
- (9) Onn, T. M.; Zhang, S. Y.; Arroyo-Ramirez, L.; Chung, Y. C.; Graham, G. W.; Pan, X. Q.; Gorte, R. J. Improved Thermal Stability and Methane-Oxidation Activity of Pd/Al₂O₃ Catalysts by Atomic Layer Deposition of ZrO₂. ACS Catal. **2015**, *5*, 5696–5701.

- (10) Mao, X. Y.; Lin, C.; Graham, G. W.; Gorte, R. J. A Perspective on Thin-Film Perovskites as Supports for Metal Catalysts. *ACS Catal.* **2020**, *10*, 8840–8849.
- (11) Cao, T. Y.; Kwon, O.; Lin, C.; Vohs, J. M.; Gorte, R. J. Two-Dimensional Perovskite Crystals Formed by Atomic Layer Deposition of CaTiO₃ on γ -Al₂O₃. *Nanomaterials* **2021**, *11*, 2207–2214.
- (12) Kwon, O.; Huang, R. J.; Cao, T. Y.; Vohs, J. M.; Gorte, R. J. Dry reforming of methane over Ni supported on LaMnO₃ thin films. *Catal. Today* **2021**, 382, 142–147.
- (13) Shen, K.; Fan, M.; Rai, R. K.; Stach, E. A.; Gorte, R. J.; Vohs, J. M. Structure and redox properties of CeMnO₃ thin films. *J. Solid State Chem.* **2023**, 323, 124055.
- (14) Shen, K.; Fan, M. J.; Kwon, O.; Viescas, A. J.; Papaefthymiou, G. C.; Gorte, R. J.; Vohs, J. M. Reversible perovskite-fluorite phase transition in alumina-supported CeFeO_x films. *J. Mater. Chem. A* **2023**, *11*, 4183–4193.
- (15) Kwon, O.; Foucher, A. C.; Huang, R. J.; Stach, E. A.; Vohs, J. M.; Gorte, R. J. Evidence for redispersion of Ni on LaMnO₃ films following high-temperature oxidation. *J. Catal.* **2022**, *407*, 213–220.
- (16) Shah, P. R.; Kim, T.; Zhou, G.; Fornasiero, P.; Gorte, R. J. Evidence for entropy effects in the reduction of ceria-zirconia solutions. *Chem. Mater.* **2006**, *18*, 5363–5369.
- (17) Herrera, G.; Chavira, E.; Jimenez-Mier, J.; Ordonez, A.; Fregoso-Israel, E.; Banos, L.; Bucio, E.; Guzman, J.; Novelo, O.; Flores, C. Structural and morphology comparison between m-LaVO₄ and LaVO₃ compounds prepared by sol-gel acrylamide polymerization and solid state reaction. *J. Alloys Compd.* **2009**, 479, 511–519.
- (18) Da Silva, J. L.; Ganduglia-Pirovano, M. V.; Sauer, J. Formation of the cerium orthovanadate CeVO₄: DFT+*U* study. *Phys. Rev. B* **2007**, *76*, 125117.
- (19) Garvie, L. A. J.; Buseck, P. R. Determination of Ce⁴⁺/Ce³⁺ in electron-beam-damaged CeO₂ by electron energy-loss spectroscopy. *J. Phys. Chem. Solids* **1999**, *60*, 1943–1947.
- (20) Lin, X. W.; Wang, Y. Y.; Dravid, V. P.; Michalakos, P. M.; Kung, M. C. Valence States and Hybridization in Vanadium-Oxide Systems Investigated by Transmission Electron-Energy-Loss Spectroscopy. *Phys. Rev. B* **1993**, *47*, 3477–3481.
- (21) Fitting Kourkoutis, L.; Hotta, Y.; Susaki, T.; Hwang, H. Y.; Muller, D. A. Nanometer scale electronic reconstruction at the interface between LaVO₃ and LaVO₄. *Phys. Rev. Lett.* **2006**, *97*, 256803.
- (22) Creaser, D. A.; Harrison, P. G.; Morris, M. A.; Wolfindale, B. A. X-Ray Photoelectron Spectroscopic Study of the Oxidation and Reduction of a Cerium(III) Oxide Cerium Foil Substrate. *Catal. Lett.* **1994**, 23, 13–24.
- (23) Pfau, A.; Schierbaum, K. D. The Electronic-Structure of Stoichiometric and Reduced CeO₂ Surfaces an XPS, UPS and HREELS Study. Surf. Sci. 1994, 321, 71–80.
- (24) Pfau, A.; Schierbaum, K. D.; Gopel, W. The Electronic-Structure of CeO₂ Thin-Films the Influence of Rh Surface Dopants. *Surf. Sci.* **1995**, 331-333, 1479–1485.
- (25) Silversmit, G.; Depla, D.; Poelman, H.; Marin, G. B.; De Gryse, R. Determination of the V2p XPS binding energies for different vanadium oxidation states (V^{5+} to V^{0+}). *J. Electron Spectrosc. Relat. Phenom.* **2004**, 135, 167–175.
- (26) Bourlier, Y.; Fregnaux, M.; Berini, B.; Fouchet, A.; Dumont, Y.; Aureau, D. XPS monitoring of SrVO₃ thin films from demixing to air ageing: The asset of treatment in water. *Appl. Surf. Sci.* **2021**, *553*, 149536.
- (27) Lin, L.; Jacobs, R.; Chen, D. Z.; Vlahos, V.; Lu-Steffes, O.; Alonso, J. A.; Morgan, D.; Booske, J. Demonstration of Low Work Function Perovskite SrVO₃ Using Thermionic Electron Emission. *Adv. Funct. Mater.* **2022**, 32, 2203703.
- (28) Janots, E.; Bernier, F.; Brunet, F.; Munoz, M.; Trcera, N.; Berger, A.; Lanson, M. Ce(III) and Ce(IV) (re)distribution and fractionation in a laterite profile from Madagascar: Insights from in situ XANES spectroscopy at the Ce $L_{\rm III}$ -edge. *Geochim. Cosmochim. Acta* **2015**, *153*, 134–148.

- (29) Shah, P. R.; Khader, M. M.; Vohs, J. M.; Gorte, R. J. A comparison of the redox properties of vanadia-based mixed oxides. *J. Phys. Chem. C* **2008**, *112*, 2613–2617.
- (30) Cordatos, H.; Ford, D.; Gorte, R. J. Simulated annealing study of the structure and reducibility in ceria clusters. *J. Phys. Chem. A* **1996**, *100*, 18128–18132.
- (31) Ghotekar, S.; Pansambal, S.; Lin, K. Y. A.; Pore, D.; Oza, R. Recent Advances in Synthesis of CeVO₄ Nanoparticles and Their Potential Scaffold for Photocatalytic Applications. *Top. Catal.* **2023**, *66*, 89–103.
- (32) Lu, G.; Song, B.; Li, Z.; Liang, H. Y.; Zou, X. J. Photocatalytic degradation of naphthalene on CeVO₄ nanoparticles under visible light. *Chem. Eng. J.* **2020**, 402, 125645.
- (33) Peyrovi, P.; Gillot, S.; Dacquin, J. P.; Granger, P.; Dujardin, C. The Activity of CeVO₄-Based Catalysts for Ammonia-SCR: Impact of Surface Cerium Enrichment. *Catal. Lett.* **2021**, *151*, 1003–1012.

TRECOMMENDED Recommended by ACS

Facile Fabrication of High-Performance Thermochromic ${\rm VO}_2\text{-Based}$ Films on Si for Application in Phase-Change Devices

Antonio J. Santos, Francisco M. Morales, et al.

MAY 30, 2023

CHEMISTRY OF MATERIALS

READ 🗹

Suppression of Strain Relaxation in VO₂/TiO₂ Multilayered Films

Binjie Chen, Hiromichi Ohta, et al.

APRIL 04, 2023

ACS APPLIED ELECTRONIC MATERIALS

READ 🗹

Strain-Induced Modulation of Resistive Switching Temperature in Epitaxial VO₂ Thin Films on Flexible Synthetic Mica

Yuta Arata, Masahiro Yoshimoto, et al.

NOVEMBER 01, 2022

ACS OMEGA

READ **C**

Structure and Optical Properties of AlN Crystals Grown by Metal Nitride Vapor Phase Epitaxy with Different V/III Ratios

Luxiao Xie, Guifeng Chen, et al.

JUNE 25, 2022

ACS OMEGA

READ 🗹

Get More Suggestions >